Journal of Alloys and Compounds 507 (2010) 201–206

Contents lists available at ScienceDirect

Journal of Alloys and Compounds

journal homepage: www.elsevier.com/locate/jallcom

Optical, magnetic and electrical investigation of cobalt ferrite nanoparticles synthesized by co-precipitation route

I.H. Gul [a,*], A. Maqsood [a], M. Naeem [b], M. Naeem Ashiq [c]

[a] Thermal Transport Laboratory, School of Chemical and Materials Engineering (SCME), National University of Sciences and Technology (NUST), H-12, Islamabad, Pakistan
[b] Department of Applied Physics, Federal Urdu University, Islamabad, Pakistan
[c] Department of Chemistry, Bahauddin Zakariya University, Multan, Pakistan

ARTICLE INFO

Article history:
Received 29 April 2010
Received in revised form 14 July 2010
Accepted 21 July 2010
Available online 30 July 2010

Keywords:
AC magnetic susceptibility
Activation energy
Electrical resistivity
Dielectric constant
Ferrite
Nanoparticles
X-ray diffraction

ABSTRACT

Aluminum substituted cobalt ferrite nanoparticles $CoFe_{2-x}Al_xO_4$ (for $x = 0.00, 0.25, 0.50$) have been synthesized by the chemical co-precipitation route. The average crystallite size was calculated using the Scherrer formula and found within 17–27 nm range. The optical absorption spectra of all the samples showed two clear electronic transitions, first is around 0.75 eV while the second at about 0.84 eV. The later is identified by means of $^4A_2 \rightarrow {}^4T_1\ (^4F)$ transition while the former is attributed to the overlapping of the $^4A_2 \rightarrow {}^4T_1\ (^4F)$ transition of the tetrahedral Co^{2+} ions and the $Co^{2+} + Fe^{3+} \rightarrow Co^{3+} + Fe^{2+}$ metal–metal charge transfer transition. The saturation magnetization at room temperatures was found to be 61.50 emu/g for pure $CoFe_2O_4$ nanoparticles, while it decreased with increasing Al^{3+} concentration up to 52.00 emu/g (for $x = 0.50$). The Curie temperature was determined from AC magnetic susceptibility measurement. It was observed that Curie temperature decreased with Al^{3+} concentration (x) and DC electrical resistivity decreased with increase in temperature. Activation energy and drift mobility have been calculated from the temperature dependent DC electrical resistivity measurements for all the samples. The variation of dielectric constant, dielectric loss and tangent loss factor for all the samples have been studied as a function of frequency in the range 600 Hz to 1 MHz at room temperature.

1. Introduction

Ferrites are a group of important magnetic materials for technological application and fundamental studies. Soft magnetic ferrite nanoparticles have critical need for the very high frequency applications such as broadband transformers, filters, antennas and microwave absorbing materials [1,2]. Many scientists have devoted their effort for studying nano-ferrite materials especially those of many technological and industrial applications such as an excellent chemical stability, high mechanical hardness, high Curie temperature, low porosity, high corrosion resistivity, magnetocrystalline anisotropy, magnetostriction, magneto-optical properties and reasonable cost [3–7]. These are used in microwave devices [8,9] due to their high resistivity, high permittivity and low losses. $CoFe_2O_4$ ferrite is a soft magnetic ceramic that has the potential to meet these requirements. The control of the dielectric behaviours as well as the magnetic properties at high frequencies has attracted much attention in recent years [10]. Since the electromagnetic properties of spinel $CoFe_2O_4$ ferrite nanoparticles are sensitive to their compositions and microstructures [11], the key to obtaining high-performance ferrites is a synthesis by a special technique. Traditional ceramic preparation methods [12,13] for nanosized spinel ferrite often suffer from uncontrolled stoichiometric poor composition, chemical inhomogenity, contamination, coarser particle size, and introduction of impurities during ball milling/grinding and high annealing temperature [14,15]. In addition, the coarse and non-uniform particles, on compacting, result in the formation of voids or low-density areas in the green compacts.

Wet chemical method such as chemical co-precipitation has overcome these drawbacks and produced ferrite nanoparticles with reproducible stoichiometric composition and desired microstructures. In chemical methods of preparation of nanosized particles with desired physical properties, the structural and chemical properties of the constituents are of prime importance. Because of mixing at molecular level, good chemical homogeneity can be achieved. Also, it allows a good control on the shape and size distribution during nanoparticles synthesis. Due to these reasons the chemical routes of preparation have emerged as a very popular synthesis tool for nanoparticles of spinel ferrites. Ferrite is one of the principal constituents of the microwave absorption materials [16], which is capable of absorbing electromagnetic radiation. We report new finding in this paper.

2. Experimental

Co-ferrite nanoparticles with nominal composition $CoFe_{2-x}Al_xO_4$ for x ranging from 0.0 to 0.5 were prepared by co-precipitating aqueous solutions of

* Corresponding author. Tel.: +92 333 5766392.
E-mail address: iftikhar_qau@yahoo.com (I.H. Gul).

0925-8388/$ – see front matter © 2010 Elsevier B.V. All rights reserved.
doi:10.1016/j.jallcom.2010.07.155

$Co(NO_3)_2{\cdot}6H_2O$, $Fe(NO_3)_3{\cdot}9H_2O$ and $Al(NO_3)_3{\cdot}9H_2O$ mixtures, respectively, in alkaline medium. The morality of the co-precipitation agent (NaOH) used was 3 mol/l. All the chemicals were of analytical grade. The solutions of $CoCl_2{\cdot}6H_2O$, $Fe(NO_3)_3{\cdot}9H_2O$ and $Al(NO_3)_3{\cdot}9H_2O$ in their stoichiometry (100 ml of 0.1 M $Co(NO_3)_2{\cdot}6H_2O$, 100 ml of 0.15 M $Fe(NO_3)_3{\cdot}9H_2O$, 100 ml of 0.05 M $Al(NO_3)_2{\cdot}9H_2O$ in the case of $CoFe_{1.5}Al_{0.5}O_4$ and similarly for the other values of x) were dissolved in distilled water with a constant stirring. The aqueous solution was heated up to 85 °C under constant stirring. The heated (85 °C) precipitating reagent (NaOH) was mixed into metal solutions, contained in a beaker, with constant stirring at 85 °C temperature. The pH of the reactions was maintained 12.0–12.5 at room temperature. The precipitates were thoroughly washed with distilled water until the washings were free from sodium and chloride ions. The product was dried in an electric oven at a temperature of 90 °C for overnight to remove water contents. The dried powder was mixed homogeneously in an agate mortar and pestle for 20 min. For pellet (13 mm diameter and 2 mm thickness) formation a load of 50 kN for 5 min was applied on each pellet. The pellets were sintered at 800 °C for 6 h and these pellets were used for magnetic and electrical measurements.

X-ray diffraction (XRD) pattern for each sample was recorded and confirmed the formation of well-defined single-phase spinel structures. XRD data were taken at room temperature using Cu Kα (λ = 1.5406 Å) radiation. The average crystallite size, D_{ave}, lattice constant, a, and measured density, ρ_m, were calculated using the standard relations [17,18].

Diffuse reflectance spectra in the wavelength range 2050–300 nm (0.6–4.1 eV) were obtained with the UV-visible Ocean Optics USB2000 fiber optic spectrophotometer. All spectra were referenced with the standard $BaSO_4$. For a more precise compression all spectra were converted to the Kubelka–Munk remission function [19] by

$$f(R_d) = \frac{(1-R_d)^2}{2R_d} = \frac{k}{s}, \quad (1)$$

where $f(R_d)$ is the Kubelka–Munk function, R_d is the diffuse reflectance from the sample, and s is the scattering coefficient. If the dependence of the scattering coefficient s on the wavelength of the incident light is neglected over the range of interest, the function $f(R)$ is directly proportional to the absorption coefficient k. The magnetometry studies were carried out in a commercial superconducting quantum interference device (SQUID) magnetometer with a field up to 2 T for the magnetization curves.

To measure the Curie temperature of the prepared samples, high temperature AC magnetic susceptibility apparatus was used. The AC magnetic susceptibility (χ) measurements for all the sample were carried out in the temperature range from 300 to 800 K using primary and secondary coil setup operating at a frequency of 270 Hz and a very low AC field (0.1 Oe) was applied parallel to the axis of a disc shaped sample. The existing AC magnetic susceptibility apparatus in the research laboratory was modified for high temperature measurements. The modified apparatus was calibrated with pure nickel prior to measurement on the samples.

Ferrites are insulator but they show semiconductor like behaviour with the rise of temperature. DC electrical resistivity for all these samples was measured by two-probe method. The DC electrical resistivity of all the samples decreased with increasing temperature according to Arrhenius equation [17]

$$\rho = \rho_0 \exp\left(\frac{\Delta E}{k_B T}\right), \quad (2)$$

where k_B is the Boltzmann constant, T is the temperature and ΔE is the activation energy, which is the energy needed to release an electron from the ion for a jump to neighbouring ion, so giving rise to the electrical conductivity.

The dielectric constant (ε') measurements were carried out in the frequency range from 600 Hz to 1 MHz at room temperature using LCR Meter Bridge (WK LCR 4275). The dielectric constant was determined from the formula

$$\varepsilon' = \frac{Cd}{\varepsilon_0 A}, \quad (3)$$

where C is the capacitance of the pellet in Farad, d is the thickness of the pellet in meter, A is the cross-sectional area of the flat surface of the pellet and ε_0 is the constant of permittivity of free space.

The dielectric tangent loss factor can be calculated using the relation

$$\tan\delta = \frac{1}{2\pi f R_p C_p}, \quad (4)$$

where δ is the loss angle, f is the frequency, R_p is the equivalent parallel resistance and C_p is the equivalent parallel capacitance.

The dielectric loss (ε'') is also measured in terms of tangent loss factor ($\tan\delta$) defined by the relation [20]

$$\varepsilon'' = \varepsilon' \tan\delta, \quad (5)$$

where ε' and $\tan\delta$ are defined above.

3. Results and discussion

Fig. 1 represents the X-ray powder diffraction patterns of the synthesized samples $CoFe_{2-x}Al_xO_4$ (for x = 0.00, 0.25, 0.50). All the samples can be indexed as the single-phase cubic spinel structure. No additional phase was detected. The average crystallite size for each composition was calculated using the Scherrer formula [9]. The lattice parameter as calculated from the observed 'd' values corresponding to the specific planes is shown in Table 1. The lattice parameter varies between 8.378 and 8.369 Å with Al^{3+} concentration. The change in lattice parameter may be due to the substitution of smaller Al^{3+} ions (0.51 Å) for large Fe^{3+} ions (0.64 Å) in the system $CoFe_{2-x}Al_xO_4$. Since smaller ions are replacing larger ones, a decrease in the lattice parameter is expected. Hence the observed behaviour of the lattice parameter can be understood. From the table, it is seen that the measured density decreased from 3.519 to 3.266 g/cm^3 with Al^{3+} concentration. This may be due to the fact that Al^{3+} has smaller atomic weight (26.98 amu) than the Fe^{3+} (55.85 amu) atoms. Similar structural behaviour was noticed by

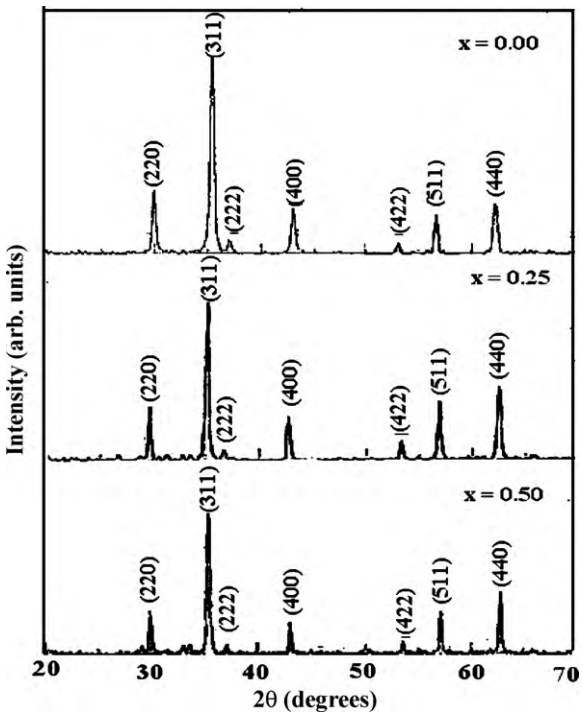

Fig. 1. Indexed X-ray pattern of $CoFe_{2-x}Al_xO_4$ (for x = 0.00, 0.25, 0.50) ferrite nanoparticles.

Table 1
Average crystallite size (D_{ave}), lattice parameter (a), lattice volume (V), X-ray density (ρ_x), measured density (ρ_m), specific surface area (S), saturation magnetization (M_s), coercively (H_c), remanence magnetization (M_r), Curie temperature (T_C), activation energy (ΔE), correlation coefficient (R), DC electrical resistivity (ρ), dielectric constant (ε'), tangent loss factor ($\tan\delta$) and dielectric loss (ε'') of $CoFe_{2-x}Al_xO_4$ ferrite nanoparticles.

Parameter	x = 0.00	x = 0.25	x = 0.50
D_{ave} (nm)	17	21	27
a (Å)	8.378(1)	8.375(6)	8.369(5)
V (Å^3)	588	587	586
ρ_x (g/cm^3)	5.270	5.006	4.987
ρ_m (g/cm^3)	3.519	3.468	3.266
M_s (emu/g)	61.5	56.5	52.0
M_r (emu/g)	11.0	13.1	20.3
H_c (Oe)	509.0	794.4	1198.2
T_C (±5 K)	672	612	572
ΔE ± 0.001 (eV)	0.559	0.487	0.507
R	0.999	0.999	0.999
ρ (×10^8 Ω cm) at 300 K ± 0.01	1.44	1.72	5.41
ε' at 1 MHz	47	42	27
$\tan\delta$ at 1 MHz	0.49	0.43	0.19
ε'' at 1 MHz	26	15	4

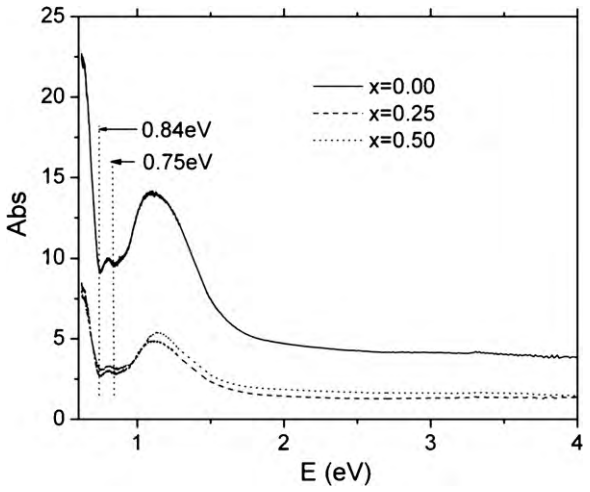

Fig. 2. UV–vis–NIR absorption spectra of $CoFe_{2-x}Al_xO_4$ (for $x = 0.00, 0.25, 0.50$) ferrite nanoparticles.

Gul and Maqsood [18] behaviour on the $CoFe_{2-x}Al_xO_4$ materials prepared by sol–gel technique.

The optical absorption spectra (extracted from reflectance measurements) for all the samples are shown in Fig. 2. The intriguing feature observed in these spectra is the appearance of characteristic absorptions one in the wavelength range of 0.75 eV, while the second at about 0.84 eV which are marked as vertical dotted lines in Fig. 2. The later absorption peak is originated from the $^4A_2 \rightarrow {}^4T_1$ (^4F) crystal field transition of the Co^{2+} ions (tetrahedral symmetry) while the former is originated from the overlapping of the $^4A_2 \rightarrow {}^4T_1$ (^4P) transition of the tetrahedral Co^{2+} and the $Co^{2+} + Fe^{3+} \rightarrow Co^{3+} + Fe^{2+}$ metal–metal charge transfer transition (MMCT) where A, P and T are generally designations of in-gap energy bands. These absorption peaks are well in agreement with the literature [21,22].

Fig. 3 shows room temperature M(H) loops of the undoped and Al^{3+} doped $CoFe_2O_4$ nanoparticles prepared under the identical conditions. The inset of Fig. 3 shows the changes in the saturation magnetization (M_s) values with the degree of Al^{3+} substitution. It is clear that the value of saturation magnetization comes out to be 61.50 emu/g at room temperature for undoped $CoFe_2O_4$ nanoparticles, which is significantly smaller than the bulk value (74.08 emu/g) [23]. Furthermore, the M_s value decreases with increasing Al^{3+} concentration from 61.50 to 52.0 emu/g for Al^{3+} concentration. In the spinel ferrites, the magnetic order is mainly due to a super exchange interaction mechanism occurring between the metal ions in the A and B sublattices. The substitution of nonmagnetic ion such as Al^{3+}, which has a preferential B site occupancy results in the reduction of the exchange interaction between A and B sites. In addition, formation of dead layer on the surface due to large surface-to-volume ratio and existence of random canting of particle surface spins at the surface [24,25] might also be the cause for the reduction of magnetization of nanoparticles.

The AC magnetic susceptibility (χ) measurements for all the samples were also carried out in the temperature range from 300 to 800 K. Fig. 4 shows the temperature dependence of AC magnetic susceptibility for $CoFe_{2-x}Al_xO_4$ ferrites. It is observed from the figure that as the Al^{3+} concentration increases, the Curie temperature, T_C decreases. According to Neel model, the A–B interaction is most dominant in ferrites, therefore, Curie temperature of ferrites are determined from the overall strength of A–B interaction [26]. The strength of A–B interaction is a function of number of $Fe^{3+}{}_A$–O^{-2}–$Fe^{3+}{}_B$ linkage, which in turn depends upon the number of Fe^{3+} ions in the formula unit and their distribution amongst A- and B-sites [26]. This results in decreasing the strength of A–B exchange interaction which leads to decrease in Curie temperature as observed experimentally (Fig. 4).

High DC electrical resistivity is a pre-requisite for high frequency applications of ferrites to counter the eddy current losses, which degrade the ferrite performance. DC electrical resistivity for all the samples were measured by two-probe method as a function of tem-

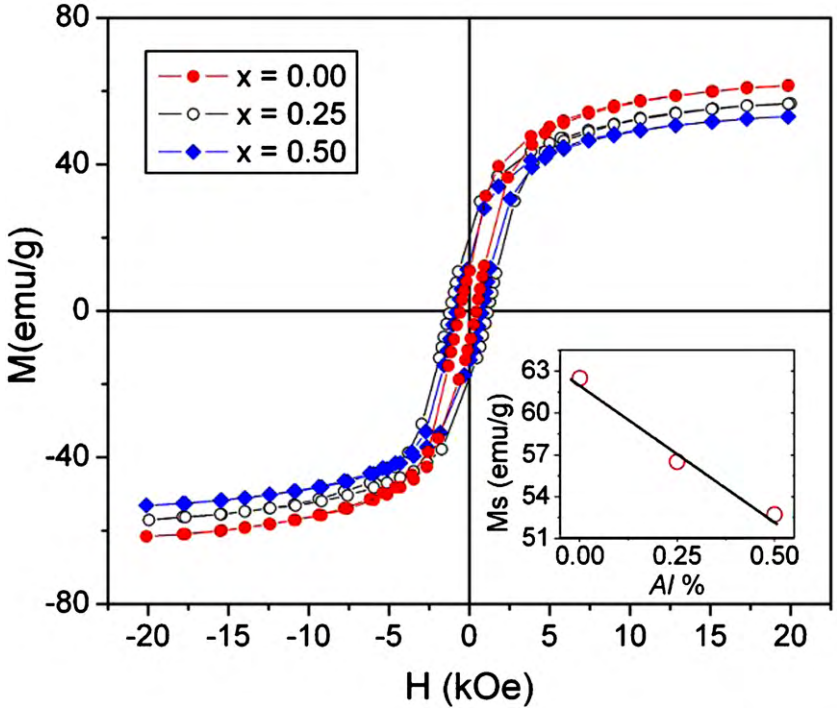

Fig. 3. Room temperature magnetization curves for undoped and Al doped $CoFe_{2-x}Al_xO_4$; inset shows the variation of saturation magnetization with Al concentration.

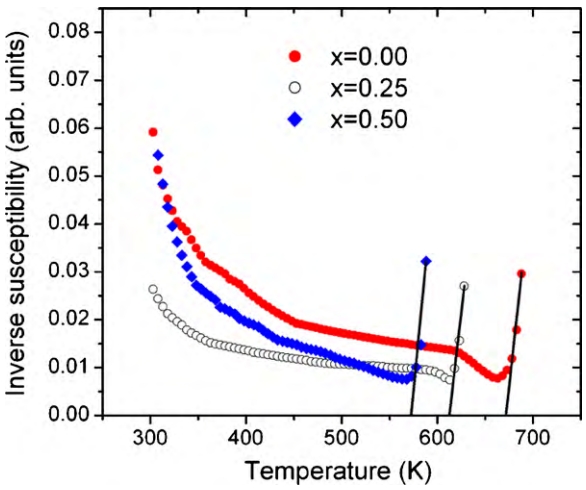

Fig. 4. Inverse AC magnetic susceptibility versus temperature of $CoFe_{2-x}Al_xO_4$ ferrite nanoparticles.

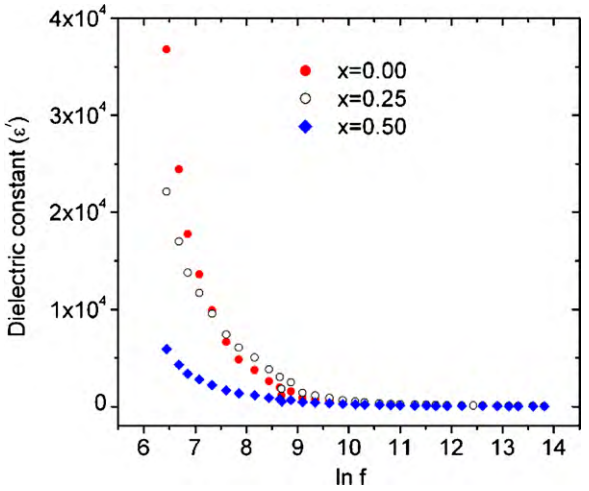

Fig. 6. Variation of dielectric constant with ln *f* of $CoFe_{2-x}Al_xO_4$ ferrite nanoparticles at room temperature.

perature and is shown in Fig. 5. From this figure, it is observed that all the samples show a linear decreasing behaviour with increasing temperature. According to Verma et al. [27] conduction in ferrites is reported to occur as a result of electron hopping between ions of the same element existing in different valence state on equivalent lattice sites. It is suggested that the conduction mechanism change linearly as temperature increases. The variation of DC electrical resistivity is explained on the basis of actual location of cation in the spinel structure. The DC electrical resistivity is observed to increase with Al^{3+} concentration. It is well known that Al^{3+} occupy octahedral site B, while Co^{2+} and Fe^{3+} ions occupy A and B sites [28,29]. Moreover, it is known that the conduction mechanism in ferrite occurs mainly through the hopping between Fe^{2+} and Fe^{3+} in the B sites. Thus, the deficient of Fe^{2+} ions with increasing Al^{3+} concentration gives further reason for the increase of the DC electrical resistivity. The Fe^{3+} ions at the A sites contribute little to conduction due to larger distances between them [27]. These values are also tabulated in Table 1.

The activation energy of each sample in the measured temperature range can be determined from the slope of the linear plots (Fig. 5) of DC electrical resistivity. The value of activation energy ranges from 0.559 to 0.507 eV. In ferrite samples, the activation

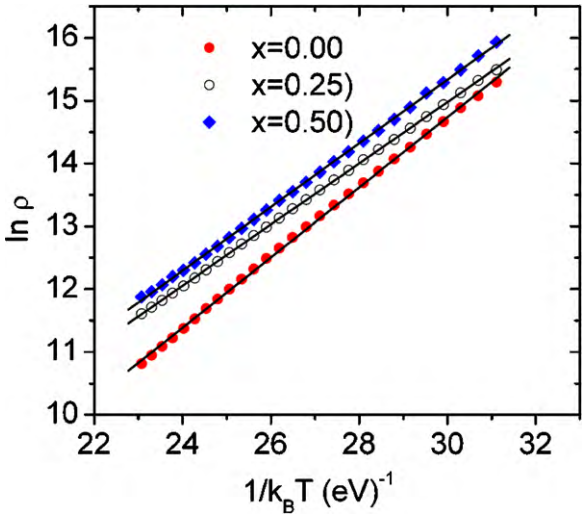

Fig. 5. Variation of DC electrical resistivity (ln ρ) with inverse temperature for $CoFe_{2-x}Al_xO_4$ ferrite nanoparticles.

energy is often associated with the variation of mobility of the charge carriers rather than with their concentration. The charge carriers are considered as localized at the ions or vacant sites and conduction occurs via a hopping process. It is noticed that the activation energy obtained in the present work for these ferrites is greater than 0.4 eV which according to Klinger [30] suggests that the conduction is due to polar on hopping. The hopping depends upon the activation energy, which is associated with the electrical energy barrier experienced by the electrons during hopping.

The dielectric constant was determined using Eq. (3). The room temperature dielectric constant as a function of frequency from 600 Hz to 1 MHz for $CoFe_{2-x}Al_xO_4$ is shown in Fig. 6. The dielectric constant decreases with successive addition of trivalent Al^{3+} concentration. The value of dielectric constant is very high at lower frequencies and decreases with the increase of frequency. At 1 MHz frequency it is very small and becomes independent of frequency. This is in agreement with earlier observations of other workers on ferrites [31,32]. A sample with high DC electrical resistivity acquires low values of dielectric constant and vice versa [33,34]. The variation in the dielectric constant of ferrites is mainly attributed to the variations in the concentration of Fe^{2+} ions [35–37]. The observed variation in dielectric constant may be understood on the basis of space charge polarization. The space charge polarization resulting from electron displacement on application of electric field and the subsequent charge build-up at the insulating grain boundary is a major contributor to the dielectric constant in ferrites. Therefore, more the number of Fe^{2+} ions in the ferrite more would be the space charge polarization expected due to the ease of electron transfer between Fe^{2+} and Fe^{3+} ions and subsequently higher the dielectric constant. The increased DC electrical resistivity obstructs the flow of space charge carriers and therefore impedes the build-up of space charge polarization. Since the DC electrical resistivity is observed to increase with Al^{3+} concentration in the present Co-ferrites, the dielectric constant is, thus expected to decrease with an increase in Al^{3+} concentration as a result of the space charge polarization.

The dielectric tangent loss factor was determined using Eq. (4). Fig. 7 shows the variation of dielectric tan δ at room temperature as a function of applied field frequency in the range 600 Hz to 1 MHz for all the samples. It can be seen that dielectric tan δ in each composition is found to decrease with increase in applied frequency. The decrease in tan δ takes place when the jumping rate of charge carriers lags behind the alternating electric field beyond a certain critical frequency. The change in dielectric loss tangent is greater at

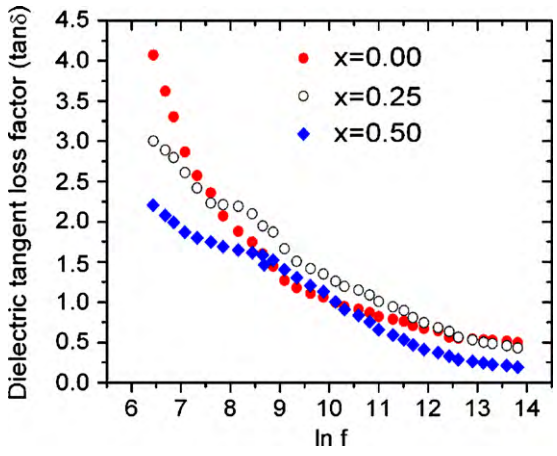

Fig. 7. Variation of dielectric loss factor with ln f of $CoFe_{2-x}Al_xO_4$ ferrite nanoparticles.

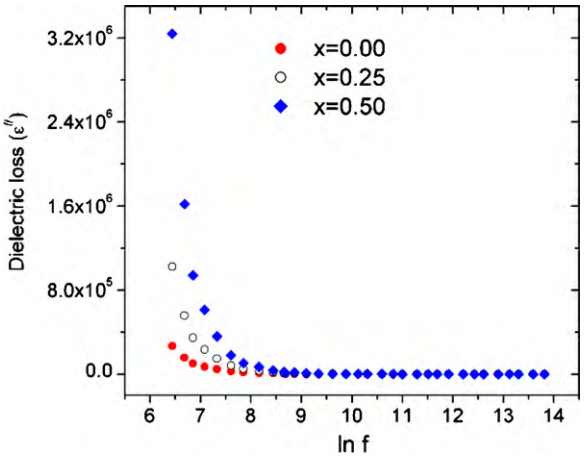

Fig. 8. Variation of dielectric loss with ln f of $CoFe_{2-x}Al_xO_4$ ferrite nanoparticles.

low frequencies and small at high frequencies for the investigated samples. The conduction in these ferrites is considered as due to the hopping of electron between divalent and trivalent ions over the octahedral sites. Rabinkin and Novikova [38] pointed out that; there is a strong correlation between the conduction mechanism and the dielectric constant behaviour (the polarization mechanism) in ferrites. From these two considerations we can see that the behaviour of tan δ with frequency is showing the expected decrease of tan δ with increasing frequency.

The dielectric loss was determined using Eq. (5). Dielectric loss is an important part of the total core loss in ferrites [39]. Hence for low core loss, low dielectric losses are desirable. The dielectric loss as a function of frequency for all the compositions is depicted in Fig. 8. The dielectric loss profiles are similar to those of the real part of dielectric constant. The increase in hopping electrons result in a local displacement in the direction of the extent electric field causing an increase in electric polarization enhances dielectric loss. Hudson [40] has shown that, the dielectric losses in ferrite is generally reflected in the conductivity measurements where the materials of highly conductivity exhibiting high losses and vice versa.

4. Conclusions

The chemical co-precipitation technique has been used for the synthesis of Co-ferrite nanoparticles $CoFe_{2-x}Al_xO_4$ (for $x = 0.00$, 0.25, 0.50) and subsequently sintered at temperature of 800 °C for 6 h. X-ray diffractograms assured the cubic spinel for all investigated samples. The average crystallite size lies within 17–27 nm range. The variation of lattice parameter is in a good agreement with the reported values [40]. The optical absorption spectra of all samples showed some intriguing features in the wavelength positions around 0.75 and 0.84 eV. These features are identified by means of transitions by the Co^{2+} via crystal field and the metal–metal charge transfer transition (MMCT) of $Co^{2+} + Fe^{3+} \rightarrow Co^{3+} + Fe^{2+}$. The saturation magnetization at room temperatures was found to be 61.50 emu/g for pure $CoFe_2O_4$ nanoparticles, while it decreases with increasing Al concentration up to 52.00 emu/g (for $x = 0.50$). Temperature dependent DC electrical resistivity decreases with increase in temperature ensuring the semiconductor like nature of the samples. The values of DC electrical resistivity at 300 K increases from 1.44×10^8 to 5.41×10^8 Ω cm, as the concentration of Al^{3+} increases from $x = 0.00$ to 0.50. The decrease in ε' and ε'' with increasing frequency for all the samples is attributed to the decrease in the polarization of the sample because the dipoles cannot follow up the field variation. The dielectric losses are reflected on the DC electrical resistivity measurements where the materials of high resistivity exhibiting low losses and vice versa. The dielectric loss decreases with Al^{3+} concentration. Low losses even at high frequencies make these samples suitable for microwave applications.

Acknowledgment

The authors would like to acknowledge Higher Education Commission (HEC) Islamabad, Pakistan and TWAS, Italy for providing financial support for this work.

References

[1] D. Cruickshank, J. Eur. Ceram. Soc. 23 (2003) 2721.
[2] M. Damnjanovic, G. Stojanovic, V. Desnica, IEEE Trans. Magn. 42 (2006) 70.
[3] J.D. Adam, S.V. Krishnaswamy, S.H. Talisa, K.C. Yoo, J. Magn. Mater. 83 (1990) 419.
[4] J.G. Lee, J.K. Park, J.Y. Oh, C.S. Kim, J. Appl. Phys. 84 (5) (1998) 2801.
[5] S.C. Petrosius, R.S. Dradgo, V. Young, G.C. Grunewald, J. Am. Chem. Soc. 115 (1993) 6131.
[6] A.K. Gupta, M. Gupta, Biomaterials 26 (2005) 3995.
[7] A.K. Giri, K. Pellerin, W. Pongsakwaswad, M. Sorescu, S. Majetich, IEEE Trans. Magn. (2000) 3029.
[8] X.H. Haung, Z.H. Chen, Scripta Mater. 54 (2006) 169.
[9] C.C. Berry, A.S.G. Curtis, J. Phys. D: Appl. Phys. 36 (2003), R 198.
[10] M. Abdun, J. Magn. Magn. Mater. 192 (1999) 121.
[11] V. Grimal, D. Autissier, L. Longuet, J. Eur. Ceram. Soc. 26 (2006) 3687.
[12] A. Verma, T.C. Goel, R.G. Mendiratta, Mater. Sci. Eng. B 156 (1999) 162.
[13] O.F. Caltun, L. Spinu, IEEE Trans. Magn. 3353 (2001) 3353.
[14] B.R. Parvatheeswara, F.O. Caltun, J. Optoelectron. Adv. Mater. 8 (2006) 995.
[15] S. Komarneni, E. Fregeau, E. Breval, J. Am. Ceram. Soc. 71 (1998) 26.
[16] A.K. Giri, E.M. Kirkpatrick, P. Moongkhhamklang, S.A. Majetich, Appl. Phys. Lett. 80 (2002) 2341.
[17] I.H. Gul, A.Z. Abbasi, F. Amin, M. Anis-ur-Rehman, A. Maqsood, J. Magn. Magn. Mater. 311 (2007) 494.
[18] I.H. Gul, A. Maqsood, J. Alloys Compd. 465 (2008) 227.
[19] Y.J. Kim, S.J. Atherton, E.S. Brigham, T.E. Mallouk, J. Phys. Chem. 97 (1993) 11802.
[20] D. Ravinder, K.V. Kumar, Bull. Mater. Sci. 24 (2001) 505.
[21] M. Abe, M. Gomi, J. Appl. Phys. 53 (1982) 8172.
[22] M. Lenglet, F. Hochu, J. Durr, J. Phys. IV 7 (1997), C1/259.
[23] M.P.G. Sandoval, A.M. Beesley, M.M. Yoshida, L.F. Cobas, J.A.M. Aquino, J. Alloys Compd. 369 (2004) 190.
[24] D.H. Han, J.P. Wang, H.L. Lou, J. Magn. Magn. Mater. 136 (1994) 176.
[25] G.M. Kale, T. Asokan, Appl. Phys. Lett. 62 (19) (1993) 2324.
[26] L. Neel, C.R. Acad. Sci. Paris 230 (1950) 275.
[27] A. Verma, O.P. Thakur, C. Prakash, T.C. Goel, R.G. Mendiratta, J. Mater. Sci. Eng. B 116 (2005) 1.
[28] A.A. Sattar, J. Mater. Sci. 39 (2004) 451.
[29] S. Singhal, J. Singh, S.K. Barthwal, K. Chanda, J. Solid State Chem. 178 (2005) 3183.
[30] M.I. Klinger, J. Phys. C8 (1975) 3595.
[31] D. Kothari, S. Phanjoubam, J.S. Baijal, J. Mater. Sci. 25 (1990) 5142.
[32] R. Manjula, V.R.K. Murthy, J. Sobhanadri, J. Appl. Phys. 59 (1986) 2929.
[33] F.G. Brockman, P.H. Dowling, W.G. Steneck, Phys. Rev. 75 (1949) 1440.

[34] D. Ravinder, B.R.P. Vijaya, Mater. Lett. 57 (2003) 4344.
[35] N. Rezlescu, E. Rezlescu, Phys. Status Solidi A 23 (1974) 575.
[36] T.S. Irvine, A. Huanosta, R. Velenzuela, A.R. West, J. Am. Ceram. Soc. 73 (1990) 729.
[37] C.G. Koops, Phys. Rev. 83 (1951) 121.
[38] L.T. Rabinkin, Z.I. Novikova, Izv. Acad. Nauk, USSR, Minsk (1960) 146.
[39] J. Zhu, K.J. Tseng, C.F. Foo, IEEE Trans. Magn. 36 (2000) 3408.
[40] A.S. Hudson, Marconi Rev. 37 (1968) 43.